

ELECTRONIC SUPPLEMENTARY INFORMATION

Charge-orbital synergistic engineering of TM@Ti₃C₂O_{1-x}B_x for highly selective CO₂ electrochemical reduction

Jiahe Peng^{a,b} Zuhao Shi^{a,b}, Jizhou Jiang^c, Peng Zhang,^d Jyh-Ping Hsu,^e Neng Li,^{a,b,c,*}

^a*State Key Laboratory of Silicate Materials for Architectures, Wuhan University of Technology, Wuhan 430070, China. E-mail: lineng@whut.edu.cn*

^b*Shenzhen Research Institute of Wuhan University of Technology, Shenzhen 518000, Guangdong, China.*

^c *School of Chemistry and Environmental Engineering, School of Environmental Ecology and Biological Engineering, Novel Catalytic Materials of Hubei Engineering Research Center, Wuhan Institute of Technology, Wuhan, 430205, China*

^d*State Center for International Cooperation on Designer Low-Carbon & Environmental Materials (CDLCEM), School of Materials Science and Engineering, Zhengzhou University, Zhengzhou 450001, Henan, China*

^e*Department of Chemical Engineering, “National Taiwan University”, Taipei, 10617*

This Supplementary Information contains:

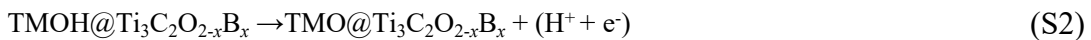
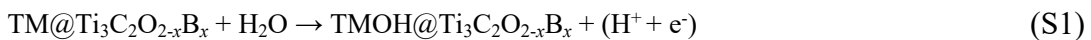
Supplementary Figures S1-S9

Supplementary Tables S1-S4

Supplementary Information contains	Pages
Pourbaix diagrams of SACs	P2
Fig. S1 PDOSs of TM@B-Ti₃C₂O₂	P3
Fig. S2 The defined area of H1 sites	P4
Fig. S3 CO₂ adsorption configuration	P4
Fig. S4 PDOS of CO₂ and TM atoms	P5
Fig. S5 ΔG of the 1st hydrogenation reaction	P6
Fig. S6 CDD of molecule adsorbed on TM@Ti₃C₂O₂	P7
Fig. S7 PDOSs of CO and TM atoms	P8
Fig. S8 Intermediates along the reaction pathway	P9
Fig. S9 CO₂ and CO adsorption configuration	P10
Table S1 Cohesive energies (Ec) of metals	P11
Table S2 G_{ads} of reduction products	P11
Table S3 Possible reaction steps of CO₂RR	P12

Pourbaix diagrams of TM@Ti₂CT_x

For an electrochemical reaction, not only AIMD simulation but also the Pourbaix diagram is necessary to evaluate the stability of materials in aqueous solution. Composed by equilibrium lines that separate two different phases, Pourbaix diagrams^{1, 2} can serve as a useful tool to identify the stable state of catalysts in water as a function of pH and applied potential. To demonstrate the stability of MXene-based SACs, their oxidation reactions (Eq. S1-2) are considered as:



The free energy change (ΔG) of these reactions are computed as:

$$\Delta G = G_{\text{TMOH@Ti}_3\text{C}_2\text{O}_{2-x}\text{B}_x} + (G_{\text{H}^+} + G_{\text{e}^-}) - G_{\text{TM@Ti}_3\text{C}_2\text{O}_{2-x}\text{B}_x} - G_{\text{H}_2\text{O}} \quad (\text{S3})$$

$$\Delta G = G_{\text{TMO@Ti}_3\text{C}_2\text{O}_{2-x}\text{B}_x} + (G_{\text{H}^+} + G_{\text{e}^-}) - G_{\text{TMOH@Ti}_3\text{C}_2\text{O}_{2-x}\text{B}_x} \quad (\text{S4})$$

Where $G_{\text{TMOH@Ti}_3\text{C}_2\text{O}_{2-x}\text{B}_x}$, $G_{\text{TM@Ti}_3\text{C}_2\text{O}_{2-x}\text{B}_x}$, $G_{\text{TMO@Ti}_3\text{C}_2\text{O}_{2-x}\text{B}_x}$ and $G_{\text{H}_2\text{O}}$ are calculated with DFT. According to the CHE model, $G_{\text{H}^+} + G_{\text{e}^-}$ can be represented as 1/2 H₂ on standard hydrogen electrode (SHE) scale:

$$G_{\text{H}^+} + G_{\text{e}^-} = 1/2G_{\text{H}_2} - eU_{\text{SHE}} - 0.059\text{pH} \quad (\text{S5})$$

Then the effect of pH and U_{SHE} can be contained as:

$$\Delta G(U, \text{pH}) = \Delta G - U_{\text{SHE}} - 0.059\text{pH} \quad (\text{S6})$$

The equilibrium line represents the values of pH and U_{SHE} when $\Delta G(U, \text{pH}) = 0$.

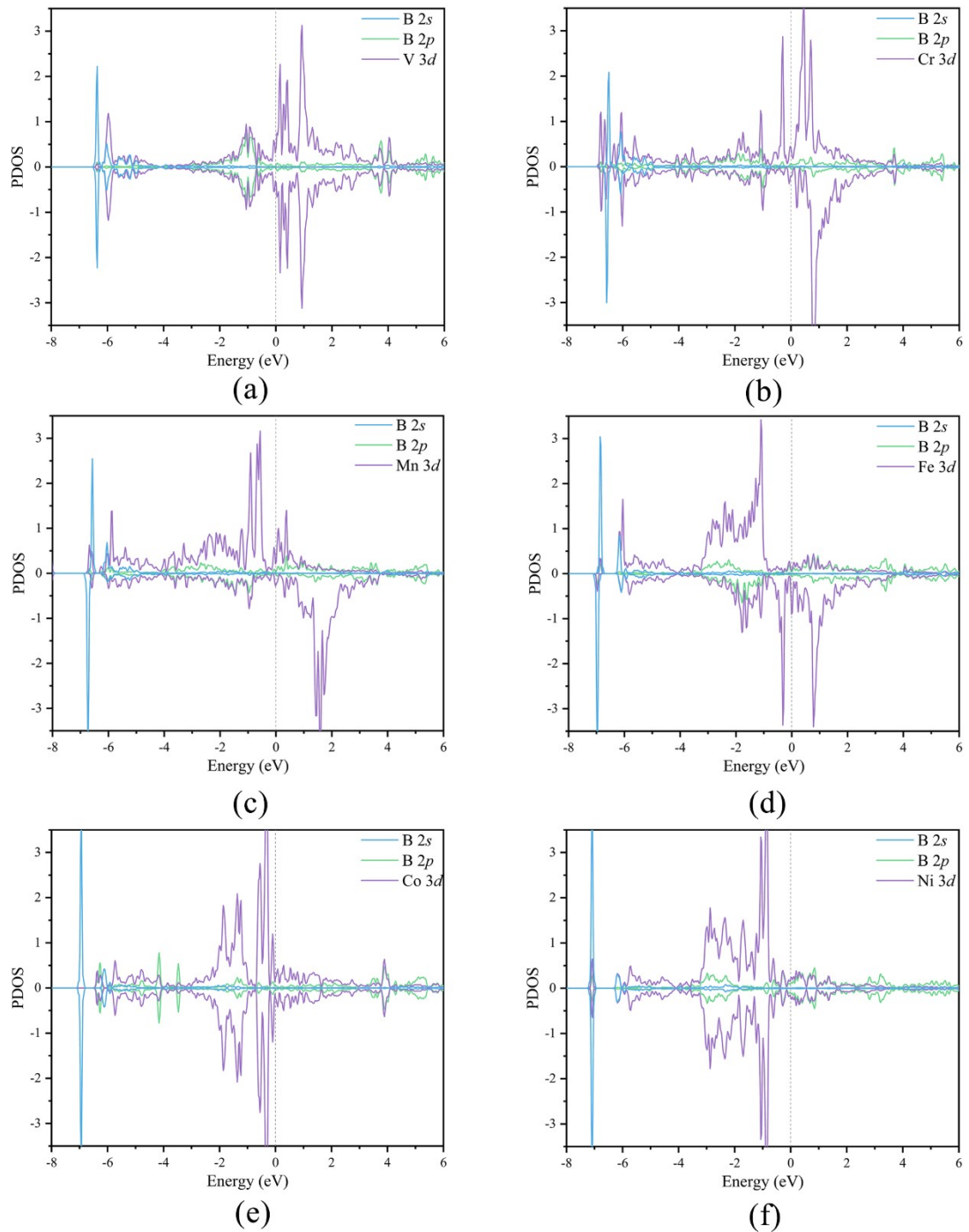


Fig. S1 DFT-calculated Projected densities of states (PDOSs) of TM@ $\text{Ti}_3\text{C}_2\text{O}_{2-x}\text{B}_x$, where TM= V, Cr, Mn, Fe, Co and Ni. The Fermi level is set to zero in black dashed line.

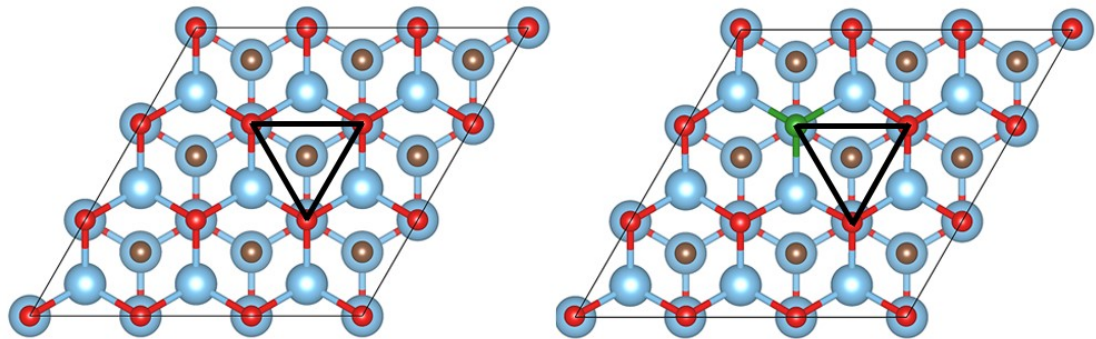


Fig. S2 The defined area of H1 sites on $\text{Ti}_3\text{C}_2\text{O}_2$ and $\text{Ti}_3\text{C}_2\text{O}_{2-x}\text{B}_x$ TM.

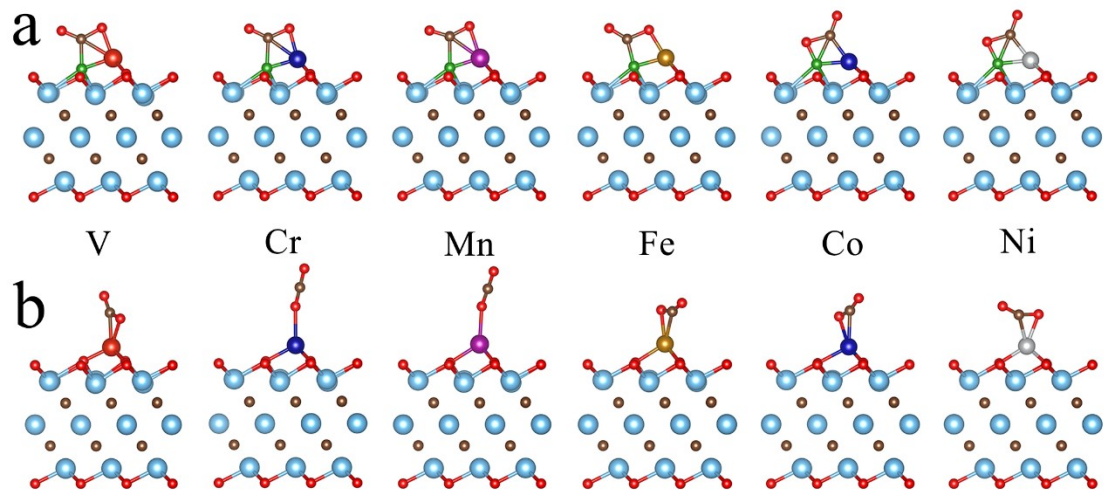


Fig. S3 Optimized geometric structures of CO_2 adsorbed on $\text{TM}@\text{Ti}_3\text{C}_2\text{O}_{2-x}\text{B}_x$ (a) and $\text{TM}@\text{Ti}_3\text{C}_2\text{O}_2$ (b).

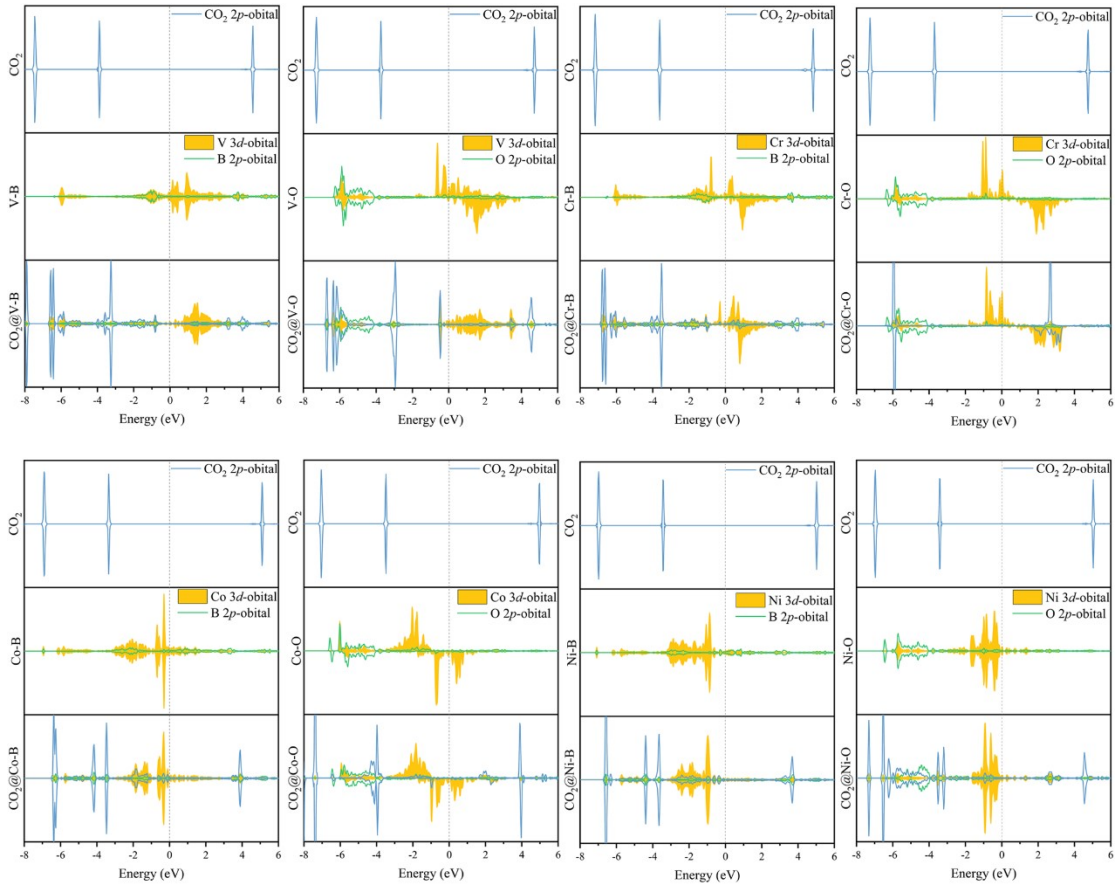


Fig. S4 The PDOS of CO_2 2p, TM 3d and coordination atoms 2p orbital before and after CO_2 adsorption on TM@ $\text{Ti}_3\text{C}_2\text{O}_{2-x}\text{B}_x$ and TM@ $\text{Ti}_3\text{C}_2\text{O}_2$.

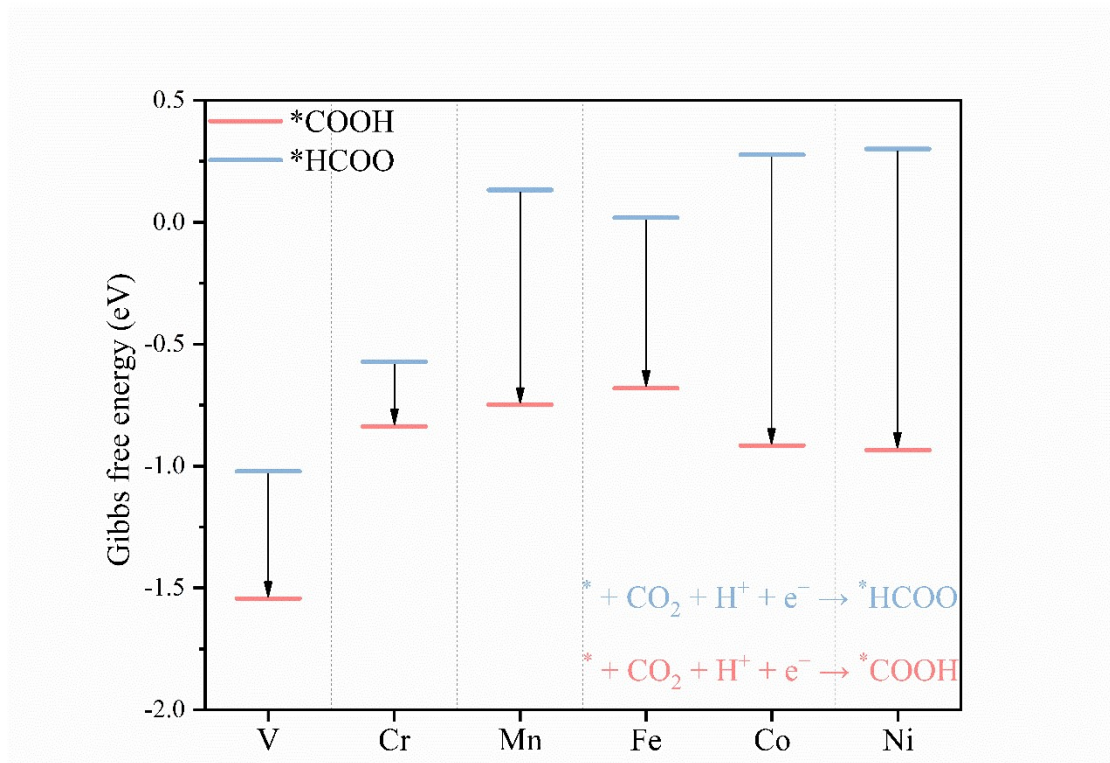


Fig. S5 Gibbs free energy changes of the 1st hydrogenation reaction for the CO₂ reduction on TM@Ti₃C₂O_{2-x}B_x.

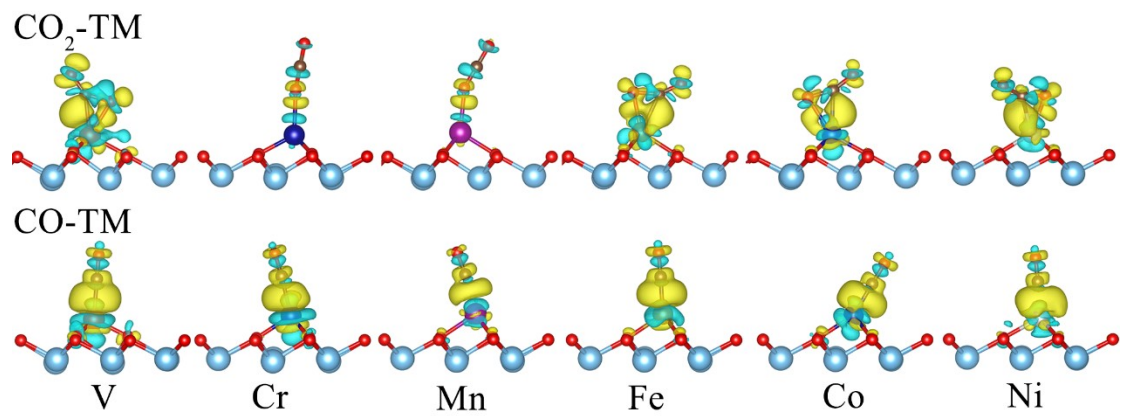


Fig. S6 The charge density differences of TM@ $\text{Ti}_3\text{C}_2\text{O}_2$ with CO_2 and CO adsorption configurations.

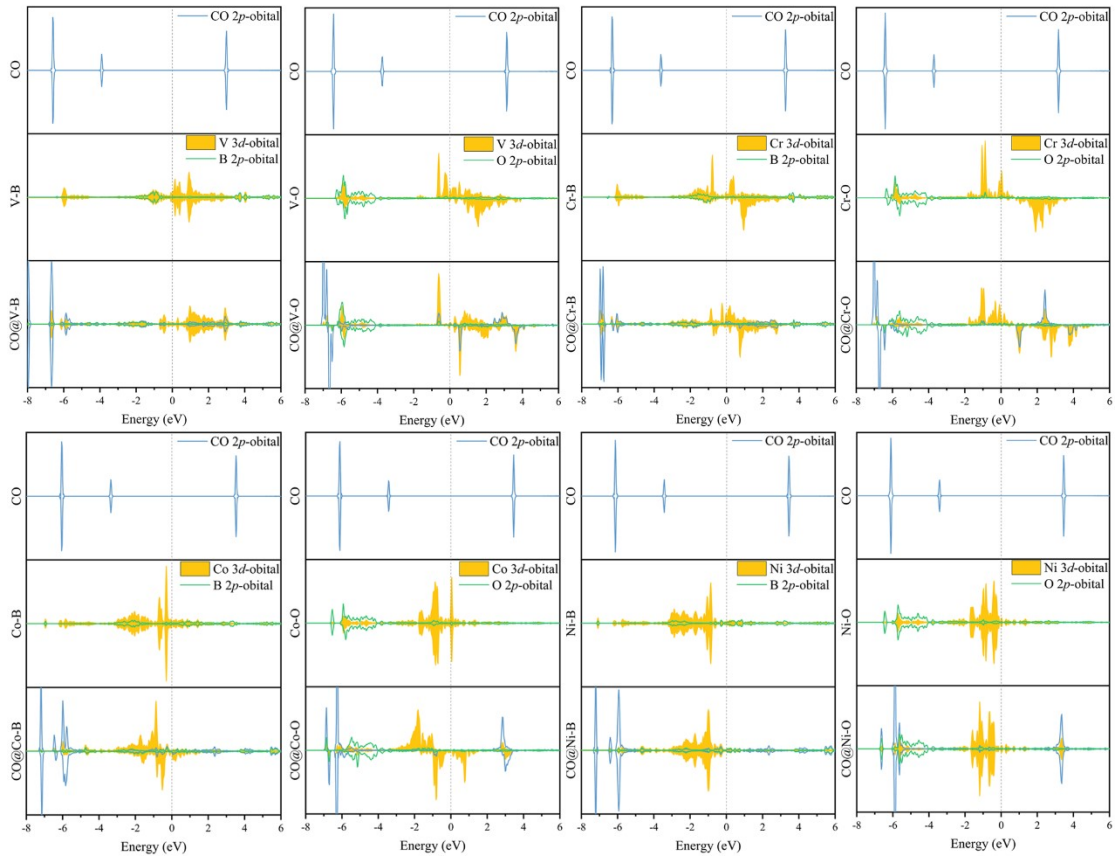


Fig. S7 The PDOS of CO 2p, TM 3d and coordination atoms 2p orbital before and after CO adsorption on TM@ $\text{Ti}_3\text{C}_2\text{O}_{2-x}\text{B}_x$ and TM@ $\text{Ti}_3\text{C}_2\text{O}_2$.

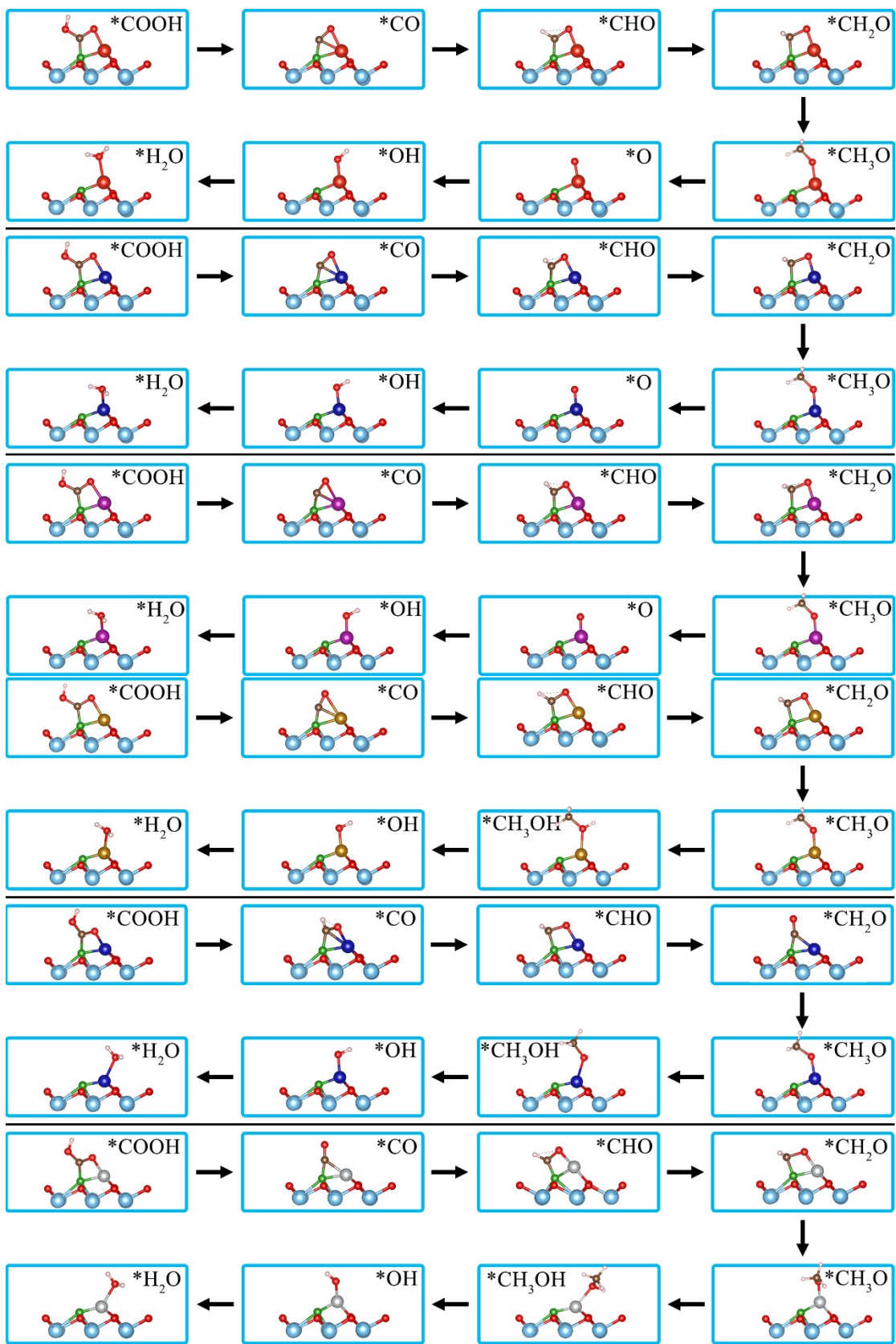


Fig. S8 DFT-optimized structures along the reaction pathway of CO₂RR.

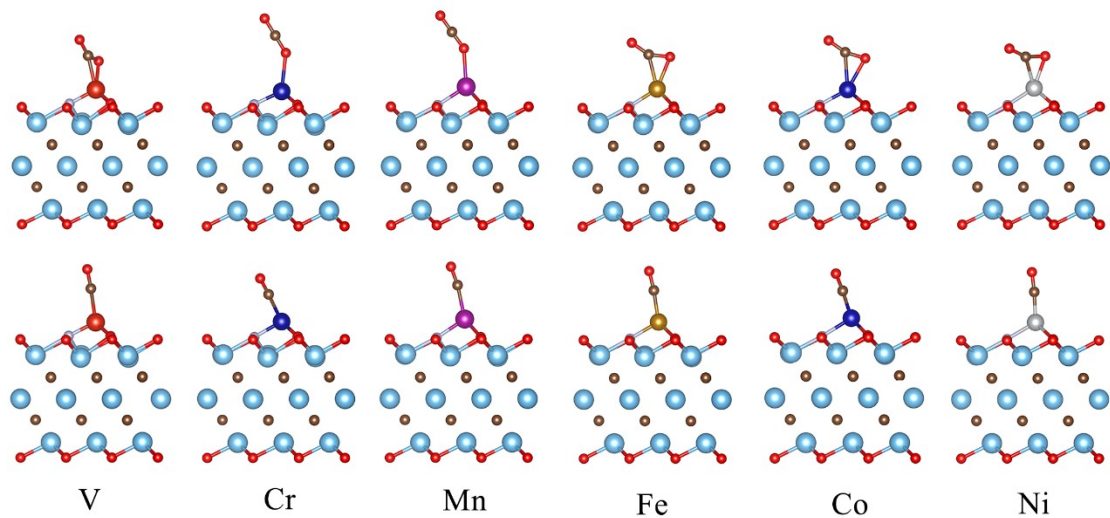


Fig. S9 Optimized geometric structures of CO_2 and CO adsorbed on $\text{TM}@\text{Ti}_3\text{C}_2\text{O}_{2-x}\text{B}_x$.

Table S1. Calculated cohesive energies (E_c) of metals and calculated binding energy - cohesive energy ($E_b - E_c$) of metal at H site.

		Ti ₃ C ₂ O _{2-x} B _x	Ti ₃ C ₂ O ₂	Ti ₃ C ₂ O _{2-x} B _x	Ti ₃ C ₂ O ₂
Metal	E_c (eV/atom) ^a	E_b (eV/atom)		$E_b - E_c$ (eV/atom)	
V	-5.62	-7.62	-5.48	-2.00	0.14
Cr	-4.04	-5.79	-3.41	-1.75	0.63
Mn	-3.49	-5.50	-3.51	-2.01	-0.02
Fe	-4.73	-5.99	-3.56	-1.26	1.17
Co	-5.01	-5.98	-3.60	-0.97	1.41
Ni	-4.85	-5.85	-3.51	-1.00	1.34

^a E_c is the intrinsic characteristic of metal and the E_c data retrieved from reference³

Table S2. Adsorption Gibbs free energy (Gads/eV) of *CO, *CH₂O and *CH₃OH reduction products on TM@Ti₃C₂O_{2-x}B_x

	CO	CH ₂ O	CH ₃ OH
V@Ti ₃ C ₂ O _{2-x} B _x	-1.8	-3.17	-1.03
Cr@Ti ₃ C ₂ O _{2-x} B _x	-0.93	-2.28	-0.47
Mn@Ti ₃ C ₂ O _{2-x} B _x	-1.10	-1.45	-0.36
Fe@Ti ₃ C ₂ O _{2-x} B _x	-0.92	-1.56	-0.58
Co@Ti ₃ C ₂ O _{2-x} B _x	-1.15	-1.54	-0.43
Ni@Ti ₃ C ₂ O _{2-x} B _x	-1.3	-1.24	-0.47

Table S3 The Gibbs free energy differences ($\Delta G/\text{eV}$) for the possible elementary hydrogenation steps of subsequent *CO reduction on TM/Ti₃C₂O_{2-x}B_x. The intermediate with red is more energetically preferred.

Hydrogenation steps	3	4	5	6	7	8
V/Ti ₃ C ₂ O _{2-x} B _x	*CHO	*CH ₂ O	*CH ₃ O	*O + CH ₄	*OH	*H ₂ O
	-0.29	-0.69	0.60	-0.24	-1.63	1.47
	*COH	*CHOH	*CH ₂ OH	*CH ₃ OH		
	2.00	0.46	2.15	0.79		
Cr/Ti ₃ C ₂ O _{2-x} B _x	*CHO	*CH ₂ O	*CH ₃ O	*O + CH ₄	*OH	*H ₂ O
	-0.30	-0.66	0.16	-0.43	-0.34	0.96
	*COH	*CHOH	*CH ₂ OH	*CH ₃ OH		
	0.73	0.67	1.55	0.91		
Mn/Ti ₃ C ₂ O _{2-x} B _x	*CHO	*CH ₂ O	*CH ₃ O	*O + CH ₄	*OH	*H ₂ O
	0.13	-0.1	0.10	-0.37	-0.41	0.23
	*COH	*CHOH	*CH ₂ OH	*CH ₃ OH		
	0.94	0.63	1.43	0.28		
Fe/Ti ₃ C ₂ O _{2-x} B _x	*CHO	*CH ₂ O	*CH ₃ O	*O + CH ₄	*OH	*H ₂ O
	0.15	-0.40	0.30	0.22	-0.96	0.15
	*COH	*CHOH	*CH ₂ OH	*CH ₃ OH		
	0.78	0.24	1.95	0.15		
Co/Ti ₃ C ₂ O _{2-x} B _x	*CHO	*CH ₂ O	*CH ₃ O	*O + CH ₄	*OH	*H ₂ O
	0.11	-0.11	0.55	0.38	-0.58	-0.18
	*COH	*CHOH	*CH ₂ OH	*CH ₃ OH		
	0.74	0.42	1.72	-0.17		
Ni/Ti ₃ C ₂ O _{2-x} B _x	*CHO	*CH ₂ O	*CH ₃ O	*O + CH ₄	*OH	*H ₂ O
	0.52	-0.08	0.68	0.85	-0.34	-0.37
	*COH	*CHOH	*CH ₂ OH	*CH ₃ OH		
	0.87	0.06	2.47	-0.64		

Table S4. DFT-predicted potential determining steps (PDS), limiting potentials (U_L) and active sites for production of CH_4 on bimetal electrocatalysts. Data of CO_2RR on other bimetal electrocatalysts were retrieved from literature.

Active site	PDS	U_L (V)	Ref.
$\text{Fe}@\text{Ti}_3\text{C}_2\text{O}_{2-x}\text{B}_x$	$^*\text{CH}_2\text{O} + \text{H}^+ + \text{e}^- = ^*\text{CH}_3\text{O}$	0.40	This work
$\text{Mn}@\text{Ti}_3\text{C}_2\text{O}_{2-x}\text{B}_x$	$^*\text{CO} + \text{H}^+ + \text{e}^- = ^*\text{CHO}$	0.51	This work
$\text{MnCu}@2\text{SV}$	$^*\text{CO} + \text{H}^+ + \text{e}^- = ^*\text{CHO}$	0.61	4
$\text{NiCu}@2\text{SV}$	$^*\text{CO} + \text{H}^+ + \text{e}^- = ^*\text{CHO}$	0.70	4
$\text{NiCo}@C_2N$	$^*\text{CHO} + \text{H}^+ + \text{e}^- = ^*\text{CHOH}$	0.25	5
$\text{Ni}_2@C_2N$	$^*\text{CO} + \text{H}^+ + \text{e}^- = ^*\text{CHO}$	0.67	5
$\text{CuMn}@BN$	$^*\text{HCOOH} + \text{H}^+ + \text{e}^- = ^*\text{CHO} + \text{H}_2\text{O}$	0.61	6
$\text{Fe}_2@BN$	$^*\text{CO} + \text{H}^+ + \text{e}^- = ^*\text{CHO}$	0.47	6
$\text{RuFe}@g\text{-C}_3\text{N}_4$	$^*\text{HCOO} + \text{H}^+ + \text{e}^- = ^*\text{HCOOH}$	0.58	7
$\text{RuCu}@g\text{-C}_3\text{N}_4$	$^*\text{HCOO} + \text{H}^+ + \text{e}^- = ^*\text{HCOOH}$	0.40	7
$\text{Mn}_2@PC_6$	$^*\text{CO} + \text{H}^+ + \text{e}^- = ^*\text{CHO}$	0.31	8
$\text{CrPd}@PC_6$	$^*\text{CO} + \text{H}^+ + \text{e}^- = ^*\text{CHO}$	0.41	8
$\text{AgCr}@N6V4$	$^*\text{CO}_2 + \text{H}^+ + \text{e}^- = ^*\text{COOH}$	0.38	9

References

- H. Niu, X. Wang, C. Shao, Z. Zhang and Y. Guo, *ACS Sustainable Chemistry & Engineering*, 2020, **8**, 13749-13758.
- K. A. Persson, B. Waldwick, P. Lazic and G. Ceder, *Phys Rev B*, 2012, **85**, 235438.
- C. Choi, S. Back, N.-Y. Kim, J. Lim, Y.-H. Kim and Y. Jung, *ACS Catal*, 2018, **8**, 7517-7525.
- Y. Li, H. Su, S. H. Chan and Q. Sun, *ACS Catal*, 2015, **5**, 6658-6664.
- Q. Huang, H. Liu, W. An, Y. Wang, Y. Feng and Y. Men, *ACS Sustainable Chemistry & Engineering*, 2019, **7**, 19113-19121.
- B. Huang, Y. Wu, Y. Luo and N. Zhou, *Chem Phys Lett*, 2020, **756**, 137852.
- S. Zhu, K. Wan, H. Wang, L.-J. Guo and X. Shi, *Nanotechnology*, 2021, **32**, 385404.
- C. Li, X. Liu, F. Xu, D. Wu, H. Xu and G. Fan, *Electrochim Acta*, 2022, **426**, 140764.
- S. Wang, L. Li, J. Li, C. Yuan, Y. Kang, K. S. Hui, J. Zhang, F. Bin, X. Fan, F. Chen and K. N. Hui, *J Phys Chem C*, 2021, **125**, 7155-7165.